Academic Journal of Applied Sciences
ISSN: 3105-0549 (Print), ISSN: 3105-0557 (Online) | Vol. 1, No. 2, 2026

Real-time Monitoring of Coaxial Fluid Reaction Rates and Analysis of Influencing Factors

Yu Li *, Shengzhao Qiao

School of Mechanical and Power Engineering, Henan Polytechnic University, Jiaozuo 454000, Henan, China

* **Corresponding author**: (Email: liyu@hpu.edu.cn)

Abstract: To enable precise control of the cross-linking process in coaxial reactive flows, this study presents an in-situ method for online measurement of the reaction rate and systematically elucidates the governing factors that influence it. The Ca^{2+} -sensitive chromogenic property of murexide is utilized to create a clear color contrast between the sol and gel layers. After elution to reveal the actual boundary of the cross-linked layer, the reaction front is superimposed on the captured flow images, and its grey-scale intensity is extracted pixel-wise. This protocol allows in-line acquisition of the cross-linked thickness at any axial position and, consequently, the calculation of the mean reaction rate. Results demonstrate that the thickness of the cross-linked layer obtained by the proposed on-line protocol deviates by only 1.09 %, fully satisfying engineering accuracy requirements. Both reactant concentrations exert a positive, co-directional influence on layer thickness and mean reaction rate, with calcium chloride concentration offering superior regulation efficacy. When the total flow rate of the coaxial reactive stream is increased while maintaining a constant flow-rate ratio, the cross-linked thickness decreases whereas the mean reaction rate rises. Conversely, extending the co-flow distance enlarges the layer thickness yet reduces the mean reaction rate.

Keywords: Coaxial extrusion, reaction flow, reaction rate, phenomenological representation, precise control.

1. Introduction

Coaxial reactive flow extrusion is a technique that enables the simultaneous deposition of two or more materials along the same longitudinal axis, facilitating the fabrication of core-shell or multi-core-shell structured capsules or fibrous materials [1-3]. This technology holds significant value and broad application prospects across diverse fields, including food science [1-2], vascularized regenerative organs [3-6], pharmaceuticals [7], sensors [8], and electronic textiles [9].

In the field of reactive flow material processing, LEE K H et al. [4] pioneered a method for fabricating hollow alginate fibers using a three-layer coaxial microfluidic system with dynamic crosslinking. In this approach, the central sodium alginate sol undergoes bidirectional diffusion crosslinking from the inner and outer calcium chloride solutions. Building on this, OH J H et al. [5] modified the coaxial reactive flow components to chitosan and sodium tripolyphosphate, successfully producing chitosan microtubes with enhanced cell adhesion properties. Further advancing the technique, LI H et al. [6] incorporated silk fibroin into sodium alginate as a bioink, while adding F127 to the calcium chloride crosslinker to induce β-sheet formation in silk fibroin, thereby creating a dual-crosslinked network. Their results demonstrated that the alginate/silk fibroin hydrogel scaffolds exhibited significantly improved mechanical properties after crosslinking.

In terms of shape formation, HUANG L Y et al. [7] utilized a coaxial reactive flow process to fabricate core-shell droplets or microcapsules for drug delivery, sustained release, and cell encapsulation. Additionally, ZHANG S Y et al. [8], researchers from Sichuan University, employed this technique to generate patterned monolayer droplets as pore-forming templates. After elution, these templates were transformed into a stretchable conductive Janus hydrogel with controllable porous structures, enabling highly sensitive monitoring of human motion. A research team from Tsinghua University, led by WANG S X et al. [9], successfully induced interfacial instability in reactive flow to achieve a whipping effect. This innovative approach enabled the fabrication of helical-channel hydrogel hollow fibers, which were subsequently utilized in wearable electronic textiles for monitoring various human movements. At Harvard Medical School, WANG D [10] printed dual-layered hydrogel tubes using a multi-channel coaxial extrusion system to mimic arterial vessels with a bilayer membrane structure. FALCONE G et al. from the University of Salerno [11] applied coaxial reactive flow printing to produce concentric geometric shapes in annular models, allowing personalized drug dosage formulation based on patient treatment plans. To ensure structural integrity when printing 3D hollow fiber constructs, GAO Q et al. from Zhejiang University [12] leveraged cross-linking kinetics, enabling adjacent hollow hydrogel fibers to fuse via residual sol on their surfaces. Building on this concept, our research team [13, 14] extended the outer needle to confine reactive flow within a more controllable laminar space, thereby regulating the reaction process. This approach ensured sufficient residual sol remained on the surface of extruded hollow fibers at the nozzle outlet to facilitate inter-fiber adhesion during deposition.

Current studies on microspheres, fibers, and 3D-printed biological structures have highlighted the need for precise control over parameters such as crosslinking layer thickness, reaction kinetics, and spatial design. However, existing research predominantly focuses on material properties and applications, with process control often relying on empirical "black-box" approaches. A critical gap remains in the systematic characterization of reaction progress and underlying mechanisms. To address this, our study proposes a novel phenomenological method for reaction rate characterization. Initially, the gray threshold of the reaction front was calibrated using the elution method, enabling real-time measurement of the cross-linked layer thickness. Subsequently, a macroscopic phenomenological expression

for the reaction rate was derived based on the cross-linked layer thickness. Finally, systematic experimental investigations were conducted to elucidate the influence of reactant concentration, solution flow rate, and co-flow distance on the reaction kinetics.

2. The Correlation Between Co-Flow Distance and Both Cross-Linked Layer Thickness and Average Reaction Rate

The principle and apparatus of coaxial reactive flow forming, as illustrated in Figure 1. The Ca^{2+} ions in the core solution diffuse radially outward, crosslinking with the shell solution. As the co-flow distance increases, the shell sol undergoes gelation, ultimately forming a hollow fiber. Figure 1b illustrates the coaxial nozzle design employed in this study, which improves upon conventional flush-tip coaxial configurations. Key modifications include: (1) Extension of the outer needle to confine the diffusion-reaction zone (i.e., reactive flow) within a more controllable laminar flow regime; (2) Implementation of a transparent PTFE outer needle for in situ reaction monitoring; and (3) Adoption of a semi-flexible inner needle structure with dynamic coaxiality adjustment capability, significantly enhancing the wall thickness uniformity of fabricated hollow fibers [15].

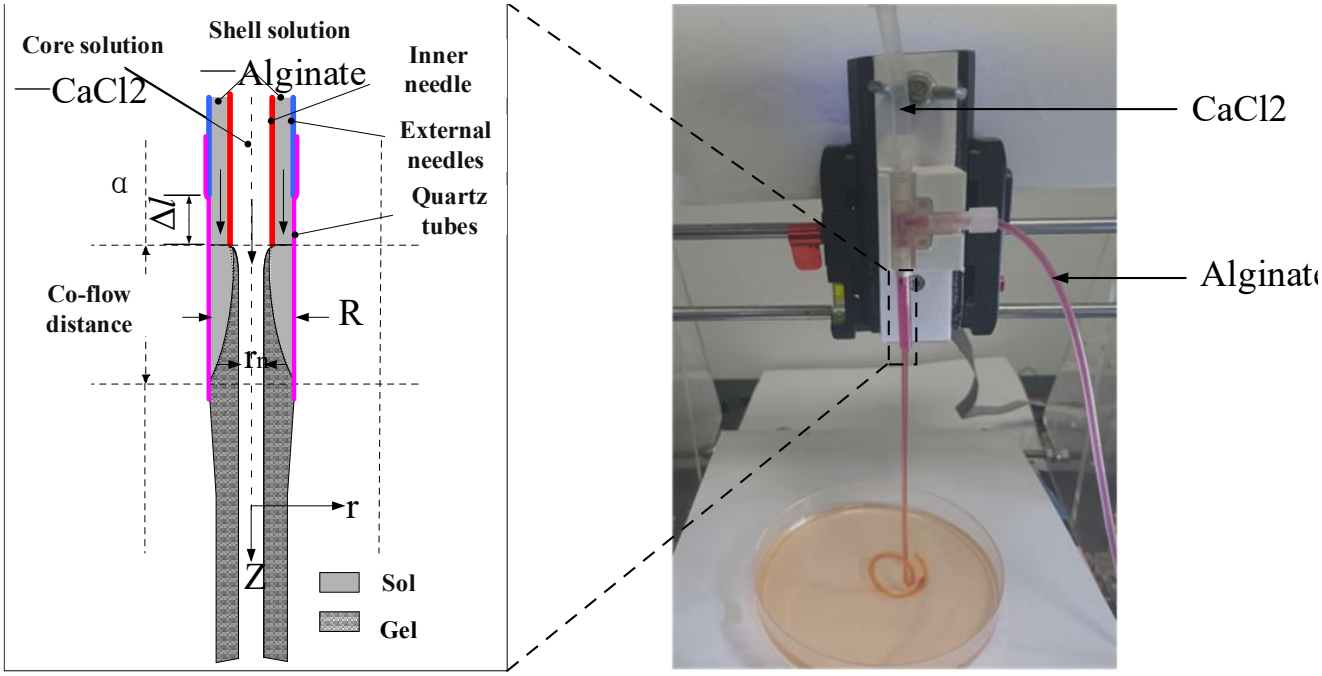

(a) Coaxial Reactive Flow Formation Mechanism (b) Coaxial Reactive Flow Fabrication Apparatus

Figure 1. Principle and device of coaxial reaction flow forming

3. Experimental and Characterization

3.1. Monitoring of Crosslinking Reaction Kinetics

As shown in Figure 3a, calcium ions (Ca^{2+}) were tracked using ammonium purpurate (murexide) as an indicator, where the yellow-colored regions distinctly marked the crosslinked calcium alginate hydrogel formation zones. Tracer elution method [16, 17] was employed to determine the actual crosslinking dimensions at the nozzle outlet due to the absence of distinct color boundaries. The separation protocol comprised: Immersion extraction: Fibers were placed in a Petri dish on a magnetic stirrer (120 rpm, 60 min) to dissolve ungelled sodium alginate from the fiber surfaces into aqueous phase, while maintaining structural integrity of the calcium alginate hydrogel (water-insoluble); Centrifugal separation: The solution was transferred to 100 mL centrifuge tubes for phase separation (3,000 rpm), followed by filtration through 300-mesh sieves and moisture removal from fibers with filter paper; Quantitative analysis: As shown in Fig. 3c, grayscale threshold calibration of the reaction front enabled subsequent in-situ image processing for direct reaction extent quantification.

During the experiment, the hollow fiber fabrication process was monitored in situ using an industrial microscope. Five representative images (Fig. 3a) were captured under identical experimental conditions (sodium alginate/calcium chloride concentrations, flow rates, and co-flow distance) during stable continuous production. These images were uniformly processed (contrast enhancement and edge sharpening) using ImageJ software (Fig. 3d). The crosslinking layer thickness was quantified by: (1) selecting a region of interest (ROI) starting from the initial crosslinking interface, (2) plotting grayscale intensity profiles across this region, and (3) establishing threshold boundaries for reaction front detection based on experimentally measured crosslinking dimensions (via elution method). The lower threshold boundary was defined by the grayscale minimum, while the upper boundary corresponded to the reaction front intensity. Binarized images were generated (Fig. 3f) for boundary distance measurement. Comparative analysis revealed only 1.09% deviation between online image-derived and elution-measured fiber dimensions (Table 1), validating both the reaction front threshold criteria and the image analysis methodology.

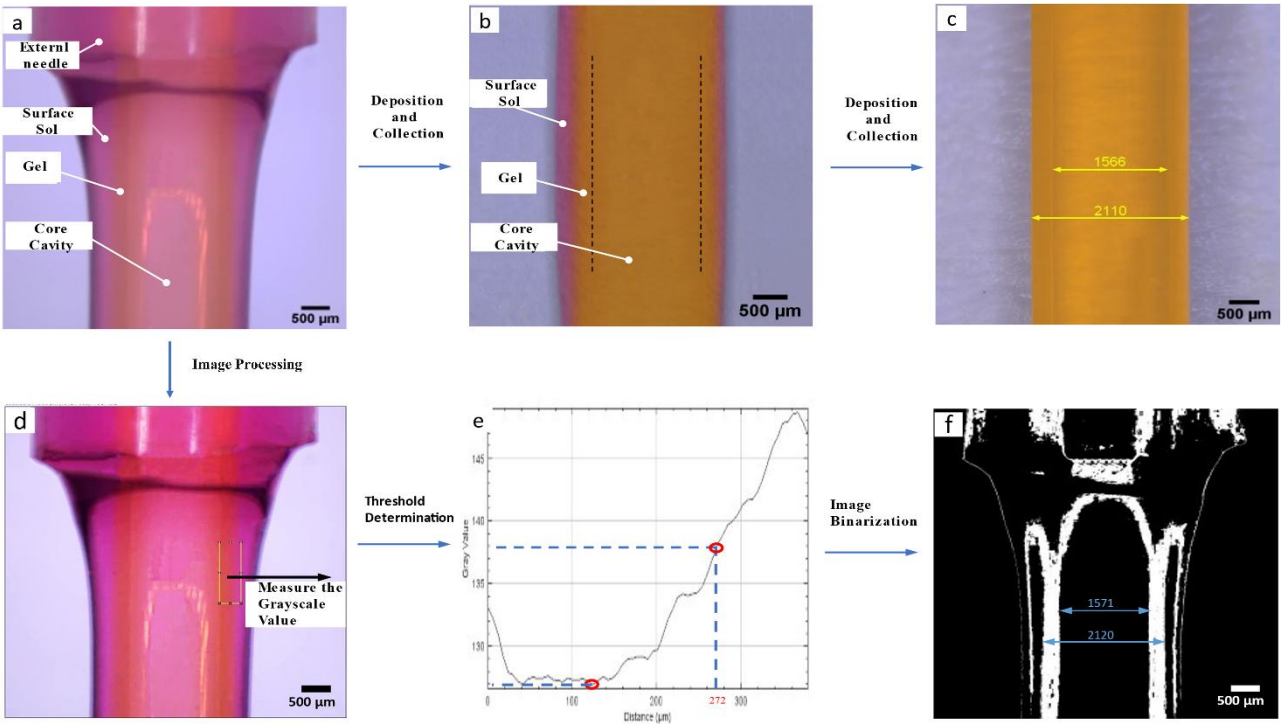

Figure 2. Determination of reaction threshold of hollow fiber crosslinking layer thickness

Table 1. Comparison of measurements by elution method and on - line identification

Scheme	Actual Crosslinking Dimension /μm	Measured Crosslinking Dimension /μm	Difference /μm
Outer Diameter Dimension	2111±15	2121±10	10
Inner Diameter Dimension	1563±15	1567±10	4
Thickness of the Crosslinked Layer	274±15	277±10	3

3.2. Effect of Co-flow Distance on Crosslinking Layer Thickness and Mean Reaction Kinetics

During coaxial reactive flow extrusion, the crosslinking reaction between alginate and Ca^{2+} is governed by both hydrodynamic effects and volumetric shrinkage from crosslinking, while the density of the colloidal medium (serving as Ca^{2+} diffusion channels) undergoes dynamic, gradient-dependent evolution. This renders the chemically measured reaction rate (in molar units) obtained from static solution bath experiments inapplicable to coaxial extrusion conditions, while also complicating reaction progress control in this process. Therefore, this study proposes a macroscopic phenomenological definition of the average reaction rate λ at a given location in the reaction flow, expressed as the ratio between the cross-linked layer thickness D of the hollow hydrogel fiber and the contact time T of coaxial biphasic flow, namely:

$$\lambda = \frac{D}{T} \tag{1}$$

Here, T represents the contact time between the coaxial biphasic flows, defined as the duration from the initiation of the sodium alginate–calcium chloride reaction to the formation of a cross-linked layer with thickness D. This time T is related to the co-flow distance S within the channel as follows:

$$T = \frac{S}{V} \tag{2}$$

Here, V denotes the average flow velocity of sodium alginate within the outer needle, which can be determined from the supply flow rate (Q_1) of the sodium alginate solution as follows:

$$V = \frac{Q_1}{\pi\left(R_1^{\,2} - r^2\right)} \tag{3}$$

Here, Q_1 represents the flow rate of the shell-phase sodium alginate solution, R denotes the inner diameter of the outer needle, and r corresponds to the hydrodynamic radius of the core-phase calcium chloride flow. These parameters can be derived from the continuity equation and Navier–Stokes equations [18] as follows:

$$r = R\sqrt{1 - \frac{m}{\sqrt{1 + \frac{Q_2}{Q_1}m} + m - 1}} \tag{4}$$

Here, Q_2 denotes the flow rate of the core-phase calcium chloride solution, and m represents the viscosity ratio between the core and shell fluids. By substituting Equations (3) and (4) into Equation (2), the average reaction rate λ at co-flow distance S can be expressed as:

$$\lambda = \frac{D}{S} \cdot \frac{Q_1}{\pi R^2 m} \left(\sqrt{1 + \frac{Q_2}{Q_1} m} + m - 1 \right) \quad (5)$$

Consequently, by combining the real-time image-based measurement of cross-linked layer thickness with process parameters including co-flow distance and flow rates of core/shell fluids, the average reaction rate λ can be quantitatively determined. Alternatively, with prior knowledge of the reaction rate profile, the co-flow distance can be precisely controlled to achieve desired cross-linked or uncross-linked layer thicknesses according to specific application requirements.

Subsequent experiments will systematically investigate the effects of reactant concentration, solution flow rate, and co-flow distance on both the cross-linked layer thickness and the average reaction rate, thereby validating the effectiveness of the proposed phenomenological reaction rate model.

4. Experiment

4.1. Materials and Methods

Sodium alginate (NaAlg): Chemical purity (CP), Sinopharm Chemical Reagent Co., Ltd. Anhydrous calcium chloride ($CaCl_2$): Analytical grade (AR), Sinopharm Chemical Reagent Co., Ltd. Ammonium purpurate (Murexide): Tianjin Damao Chemical Reagent Factory.

A predetermined quantity of sodium alginate (NaAlg) powder and ammonium purpurate tracer was accurately weighed using an analytical balance and dissolved in deionized water to prepare NaAlg solutions at concentrations of 3%, 3.5%, 4%, and 4.5% (w/v). The mixtures were homogenized using a thermostatic magnetic stirrer at room temperature (120 rpm) for 10 h, followed by additional stirring for 3 h. Subsequently, the solutions were allowed to stand for 6 h to eliminate entrapped air bubbles.

The experimental setup primarily consisted of the following instruments: an electronic balance (Model AB104-N, Shanghai Puchun Measurement Instrument Co.), a thermostatic magnetic stirrer with heating capability (Model H01-1B, Shanghai Meiyinpu Instrument Co.), an industrial microscope (Model BC4800, BoCheng Electronic Technology Co.), and a microinjection pump (Model XMSP-1C, Nanjing Ximai Nanotechnology Co., Ltd.).

4.2. Experimental Platform Establishment

Figure 3 presents the integrated coaxial reactive flow system for hollow fiber fabrication, comprising: (1) precision syringe pumps for controlled fluid delivery, (2) an MKS motion control card for system automation, (3) an industrial microscope for in situ observation, and (4) a 3D-printed modular fixture for component alignment. The industrial microscope was horizontally oriented, with focusing achieved through precise X-Y axis movements controlled by the 3D printing platform. A dual-channel precision syringe pump system was employed to co-extrude sodium alginate sol (shell layer) and calcium chloride solution (core layer). The extruded hollow fibers were collected in a deionized water-filled Petri dish, establishing an aqueous receiving environment. During experiments, the extrusion rates of both syringe pumps were precisely controlled via an MKS motion control card through custom-developed host computer software, enabling synchronized delivery of core/shell solutions.

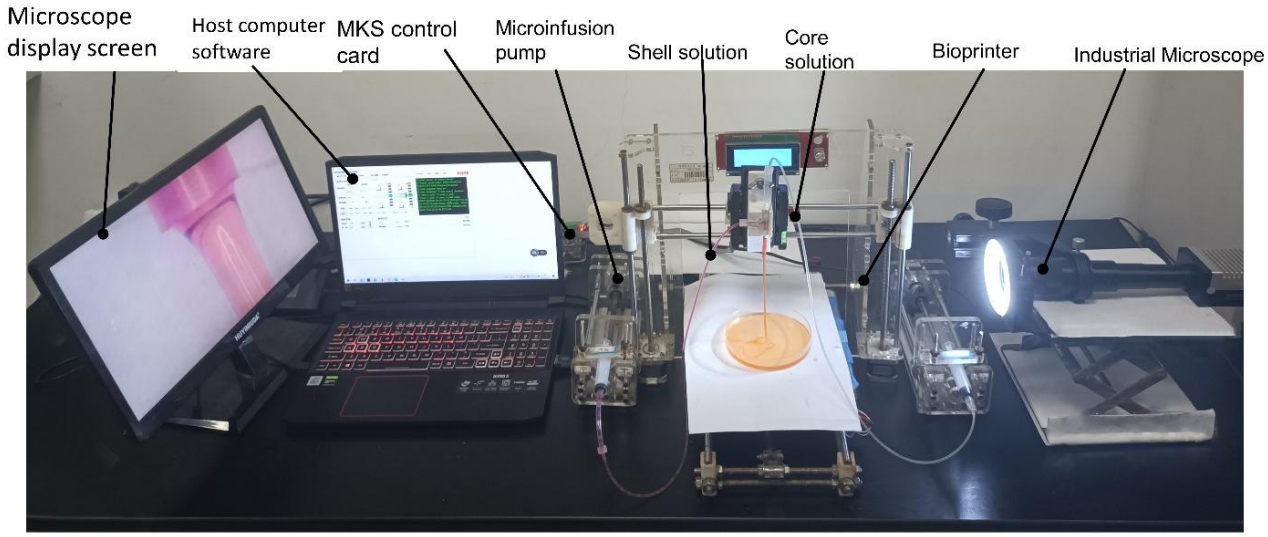

Figure 3. Online monitoring platform

5. Results and Discussion

5.1. The Effect of Reactant Concentration on Cross-Linking Layer Thickness and Average Reaction Rate

The flow rates of sodium alginate and calcium chloride solutions were set at 0.6 mL/min and 0.3 mL/min, respectively, to investigate the co-flow behavior at a coaxial reaction distance of 40 mm.

When the sodium alginate concentration was fixed at 4 wt%, both the cross-linked layer thickness and average reaction rate of the hollow fibers increased significantly with increasing calcium chloride concentration, showing a positive correlation. Specifically, the cross-linked layer thickness increased from 169 μm to 313 μm (Δ144 μm), while the average reaction rate rose from 224 μm/min to 414 μm/min (Δ190 μm), as illustrated in Fig. 4a.

At a fixed calcium chloride concentration of 5 wt%, both the cross-linked layer thickness and average reaction rate of hollow fibers increased with rising sodium alginate concentration. The cross-linked layer thickness grew from 251 μm to 282 μm (Δ31 μm), while the average reaction rate increased from 332 μm/min to 374 μm/min (Δ42 μm), showing a relatively slow growth trend as presented in Fig. 4b.

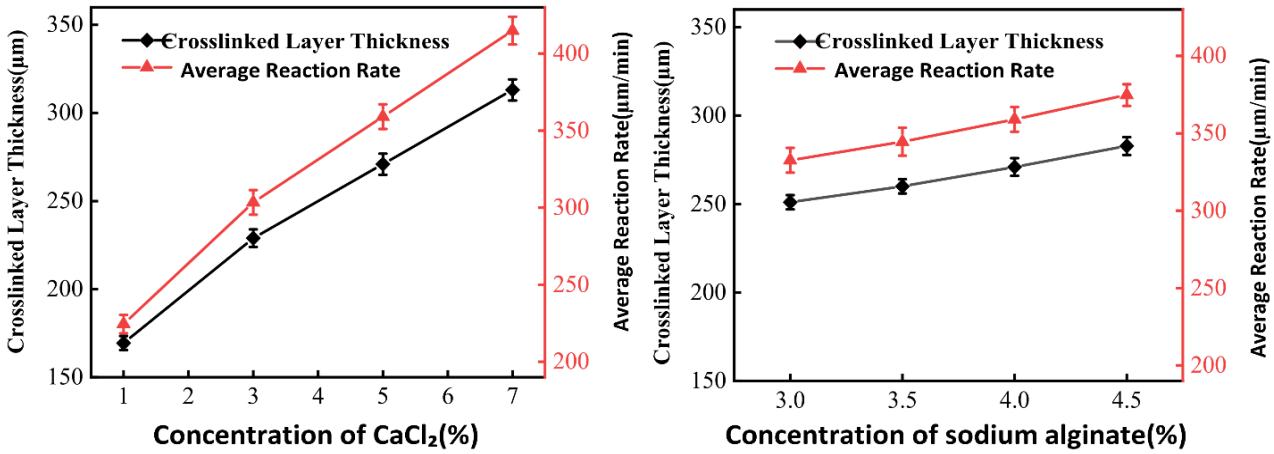

(a) The influence law of calcium chloride concentration (b) The influence law of sodium alginate concentration

Figure 4. Effect of reactant concentration on crosslinking layer thickness and average reaction rate

The experimental results demonstrate a positive correlation between sodium alginate concentration and cross-linked layer thickness, indicating an extended radial diffusion distance of Ca2+ ions. The increased sodium alginate concentration enhances the attraction effect on calcium ions, thereby facilitating their diffusion-reaction process. However, it should be noted that water serves as the essential medium for calcium ion diffusion-reaction, and the elevated sodium alginate concentration leads to reduced water content and increased gel density, which inevitably retards the diffusion-reaction rate. Consequently, the impact of sodium alginate concentration on calcium ion diffusion-reaction rate represents a competitive balance between these two opposing effects. The experimental reveal that the average reaction rate increases with sodium alginate concentration, suggesting that the inhibitory effect of gel density on Ca2+ diffusion is less dominant in this competition.

Furthermore, the concentration increase of both reactants (calcium chloride and sodium alginate) contributes to enhanced reaction rates. However, the concentration range of sodium alginate this process is relatively limited: concentrations below 3% fail to ensure adequate mechanical properties, while concentrations exceeding 5% result in poor flow characteristics and extrusion difficulties, with only approximately 30 μm variation in cross-linked layer thickness. In contrast, calcium chloride concentration can be adjusted within a broader range (1%-7%), resulting in a significant difference of approximately 140 μm in cross-linked layer thickness. Therefore, among the two reactants, calcium chloride concentration demonstrates superior controllability in regulating the reaction rate.

5.2. The Influence of Solution Flow Rate on Cross-linking Layer Thickness and Average Reaction Rate

Since the flow rate ratio affects the initial two-phase flow morphology [9], we fixed the sodium alginate-to-calcium chloride flow rate ratio at 2:1 and tested four different feed combinations (Table 2) to investigate how increasing the inner and outer flow rates influences cross-linking layer thickness and average reaction rate.

At a calcium chloride ($CaCl_2$) concentration of 5 % and alginate and $CaCl_2$ solution concentrations of 4 % and 5 %, respectively, the effect of shell–core flow rate on the hydrogel layer thickness and average reaction rate was investigated over a coaxial distance of 40 mm (Fig. 5). The results indicate that increasing the flow rates of both solutions leads to a monotonic decrease in the cross-linked layer thickness, coupled with a pronounced increase in the average reaction rate.

Table 2. Core and shell solution flow rate parameters(ml/min)

Combination / Materials	I	II	III	IV
Sodium alginate	0.4	0.6	0.8	1.0
Calcium chloride	0.2	0.3	0.4	0.5

At a calcium chloride ($CaCl_2$) concentration of 5 % and alginate and $CaCl_2$ solution concentrations of 4 % and 5 %, respectively, the effect of shell–core flow rate on the hydrogel layer thickness and average reaction rate was investigated over a coaxial distance of 40 mm (Fig. 5). The results indicate that increasing the flow rates of both solutions leads to a monotonic decrease in the cross-linked layer thickness, coupled with a pronounced increase in the average reaction rate.

This behaviour can be rationalized as follows. Although the four investigated flow-rate pairs share the same initial inner diameter (i.e., identical fluid flow-rate ratios), the residence time available for radial Ca^{2+} diffusion and subsequent ionic cross-linking diminishes with increasing flow rate over the fixed 40 mm coaxial distance. Consequently, the hydrogel layer becomes thinner as the flow rate rises. Despite the reduction in layer thickness, the accompanying reduction in residence time is proportionally greater, yielding a markedly higher average reaction rate. These observations align with the general predictions of laminar diffusion–reaction theory [9, 19], which states that convective transport dominates over both diffusion and reaction in such systems. Specifically, higher shell and core velocities generate steeper velocity gradients, thereby intensifying the local mass-transfer fluxes and accelerating the consumption (or generation) of Ca^{2+}, alginate, and calcium-alginate gel within the reaction zone.

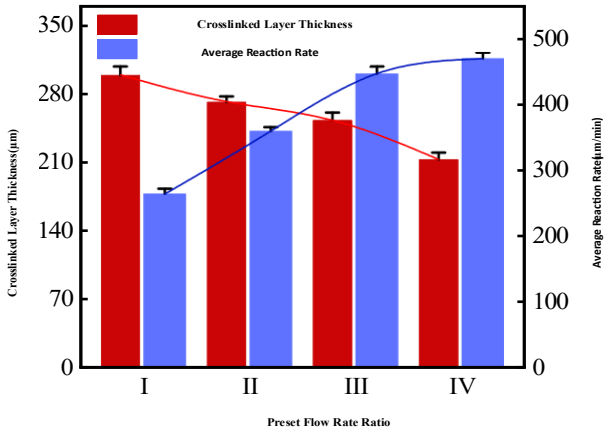

Figure 5. Effect of solution flow rate on crosslinking layer thickness and average reaction rate

5.3. Effects of Co-flow Distance on Cross-linked Layer Thickness and Average Reaction Rate

Under fixed concentrations (4% sodium alginate and 5% $CaCl_2$) and flow rates (0.6 mL/min and 0.3 mL/min, respectively), increasing the co-flow distance (by extending the outer needle length) led to thicker cross-linked layers but slower average reaction rates in the hollow fibers, as shown in Fig. 6. As the co-flow distance increases, Ca^{2+} ions have more time to diffuse radially, leading to prolonged cross-linking reactions between the core and shell solutions, thereby increasing the cross-linked layer thickness. However, the concentration gradient of Ca^{2+} decreases with longer co-flow distances, and the accumulated gel layer progressively hinders further ion diffusion. Consequently, although the total cross-linking thickness continues to grow, the rate of increase slows down due to reduced diffusion efficiency. This results in a declining average reaction rate, despite the overall thickening of the gel layer.

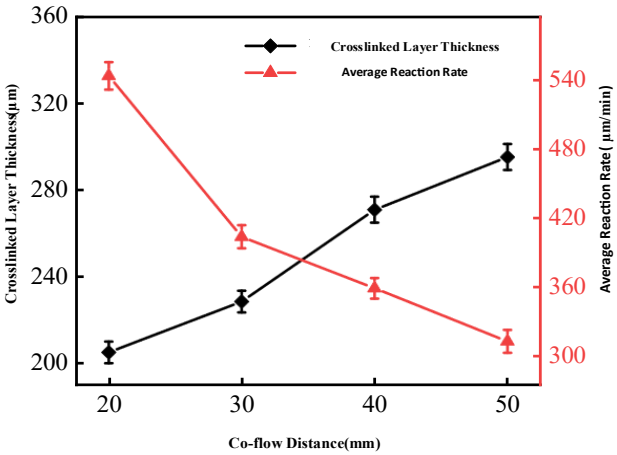

Figure 6. Effect of common-flow distance on crosslinking layer thickness and average reaction rate

5.4. Discussion

Equation (5) presented in this study establishes a comprehensive relationship among reaction rate, cross-linked layer thickness, co-flow distance, and coaxial fluid flow rate, enabling the calculation of any unknown parameter from the known variables. For instance, when fabricating fibers through reactive flow printing to achieve specific geometric structures, maintaining a certain thickness of uncross-linked layer is essential to ensure adequate surface adhesion of the fibers. In this context, the uncross-linked layer thickness can be precisely controlled through the co-flow distance, which serves as a crucial reaction space parameter. The methodology involves two sequential steps: first, obtaining the average reaction rate curve through in situ recognition of cross-linked layer thickness, combined with nozzle co-flow distance and core-shell fluid flow rates; second, determining the required co-flow distance through interpolation based on the desired cross-linked or uncross-linked layer thickness. It should be noted that the co-flow distance in this context specifically refers to the two-phase co-flow distance within the nozzle.

Compared with the diffusion-reaction theoretical model, the phenomenological average reaction rate defined in this study demonstrates consistent influence patterns with the general reaction rate in terms of fluid velocity field and chemical concentration, thereby validating the effectiveness of this phenomenological parameter. For coaxial reactive flow processes, microscopic quantitative measurement of chemical reaction rates presents significant challenges. The average reaction rate defined in this study directly correlates with the cross-linked layer thickness, which is a critical engineering parameter, thus facilitating precise control of the reaction progress in coaxial reactive flow systems.

While quantitative analysis based on image processing has been well established [20, 21], this study employed a novel approach by tracking Ca^{2+} ions using ammonium purpurate as an indicator. Through elution method calibration of grayscale thresholds at the reaction front (cross-linking boundary), we achieved real-time extraction of cross-linking thickness and phenomenological calculation of average reaction rate. Experimental validation demonstrated a measurement error of merely 1.09%, meeting engineering application requirements.

6. Summary and Conclusions

To address the precise control requirements of coaxial flow reaction systems in terms of cross-linking thickness modulation, reaction rate regulation, and spatial configuration design, this study proposes a novel phenomenological characterization method for reaction kinetics. Through systematic experimentation, we have elucidated the influence mechanisms of critical parameters including reactant concentrations, solution flow rates, and co-flow distance on the reaction dynamics.

1) The increase in reactant concentration enhances both the average reaction rate and cross-linking layer thickness. Specifically, the sodium alginate concentration exhibits a dual effect on calcium ion diffusion—promoting cross-linking at lower concentrations while introducing diffusion resistance at higher levels, resulting in a moderate increase in reaction kinetics and layer thickness. In contrast, calcium chloride concentration demonstrates a more pronounced influence, offering a wider adjustable range for controlling the cross-linking process.

2) In the fixed flow rate ratio experiments, the cross-linked layer thickness decreased while the average reaction rate increased with increasing solution flow velocity. Phenomenologically, this can be attributed to the reduction in cross-linking time being more significant than the decrease in layer thickness. These observations are consistent with the general principles described by the laminar flow diffusion-reaction equation, wherein a steeper velocity gradient enhances the reaction quantities of calcium ions, sodium

alginate, and calcium alginate gel per unit time.

3) With increasing co-flow distance, the hollow fiber cross-linking thickness exhibited progressive growth while the average reaction rate demonstrated a gradual decline. This phenomenon can be attributed to two competing mechanisms: (1) the extended residence time at longer co-flow distances permits more complete Ca^{2+} diffusion, thereby enhancing cross-linking layer formation; (2) the concomitant reduction in calcium ion concentration gradient, combined with the cumulative diffusion barrier effect of the developing gel layer, progressively impedes the reaction kinetics.

4) The phenomenological average reaction rate, calculated from in situ measurements of cross-linked layer thickness, exhibits consistent influence patterns with the general reaction rate in terms of fluid velocity field and chemical concentration. This consistency provides substantial evidence for the validity of the phenomenological definition proposed in this study.

References

[1] Qiao D L, Hu W T, Wang Z, et al. Food structuring using microfluidics: Updated progress in fundamental principles and structure types [J]. Journal of Food Engineering, 2024, 360: 111703. https://doi.org/10.1016/j.jfoodeng.2023.111703

[2] Vancauwenberghe V, Verboven P, Lammertyn J, et al. Development of a coaxial extrusion deposition for 3D printing of customizable pectin-based food simulant [J]. Journal of Food Engineering, 2018, 225:42-52. https://doi.org/10.1016/j.jfoodeng.2018.01.008

[3] Li S, Jin J L, Zhang C R, et al. 3D bioprinting vascular networks in suspension baths [J]. Applied Materials Today, 2023, 30:101729. https://doi.org/10.1016/j.apmt.2022.101729

[4] Lee K H, Shin S J, Park Y, et al. Synthesis of Cell-Laden Alginate Hollow Fibers Using Microfluidic Chips and Microvascularized Tissue-Engineering Applications [J]. Small, 2009, 5(11):1264-1268. https://doi.org/10.1002/smll.200801667

[5] Oh J, Kim K, Won S W, et al. Microfluidic fabrication of cell adhesive chitosan microtubes [J]. Biomedical Microdevices, 2013, 15(3):465-472. https://doi.org/10.1007/s10544-013-9746-z

[6] LI H, LI N N, ZHANG H, et al. Three-Dimensional Bioprinting of Perfusable Hierarchical Microchannels with Alginate and Silk Fibroin Double Cross-linked Network [J]. 3D Printing and Additive Manufacturing, 2020, 7(2):78-84. https://doi.org/10.1089/3dp.2019.0115

[7] HUANG L Y, WU K, CAI S H, et al. Understanding the microfluidic generation of double emulsion droplets with alginate shell [J]. Colloids and Surfaces B-Biointerfaces, 2023, 222: 113114. https://doi.org/10.1016/j.colsurfb.2022.113114

[8] Zhang S Y, Pan D W, Fan H D, et al. Stretchable conductive Janus hydrogel with controllable porous structures for high-performance strain sensing [J]. Journal of Polymer Science, 2023, DOI: 10.1002/pol.20230502. https://doi.org/10.1002/pol.20230502

[9] Wang S X, Chen Y J, Pei D F, et al. Rifled microtubes with helical and conductive ribs for endurable sensing device [J]. Chemical Engineering Journal, 2023, 465: 142939. https://doi.org/10.1016/j.cej.2023.142939

[10] Wang D, Maharjan S, Kuang X, et al. Microfluidic bioprinting of tough hydrogel-based vascular conduits for functional blood vessels [J]. Science advances, 2022, 8(43): eabq6900. DOI: 10.1126/sciadv.abq6900

[11] Falcone G, Saviano M, Aquino R P, et al. Coaxial semi-solid extrusion and ionotropic alginate gelation: A successful duo for personalized floating formulations via 3D printing [J]. Carbohydrate Polymers, 2021, 260:117791. https://doi.org/10.1016/j.carbpol.2021.117791

[12] Gao Q, He Y, Fu J Z, et al. Coaxial nozzle-assisted 3D bioprinting with built-in microchannels for nutrients delivery [J]. Biomaterials, 2015, 61:203-215. https://doi.org/10.1016/j.biomaterials.2015.05.031

[13] Li Y, Liu Y Y, Jiang C, et al. A reactor-like spinneret used in 3D printing alginate hollow fiber: a numerical study of morphological evolution [J]. Soft Matter, 2016, 12(8): 2392 - 2399. https://doi.org/10.1039/C5SM02733K

[14] Li Y, Shi J G, Bian P Y, et al. The permeability regulation method of calcium alginate hollow fibers based on the interfacial polarity [J]. Journal of Materials Science, 2022, 57: 22006–22018. 10.1007/S10853-022-08013-X

[15] Shen Y B, Wang S H, Yang Y Q, et al. The invention relates to a semi-flexible self-centering coaxial sprinkler head [P]. China Patent: ZL201921718292.7, 2020-10-30.

[16] Meng Q Y, Liu Z H, Xu M Y, et al. Extraction and analysis of sargassum hemiphyllum polysaccharides [J]. Spectroscopy and SpectralAnalysis, 2004, 24(12):1560-1562.

[17] Chen Y, Xu Y, Feng Y Y. Optimizing extraction process of heavy metals in fly ash using saponins by response surface methodology [J]. CIESC Journal, 2014, 65(02): 701-710.

[18] Khrennikov A Y, Kochubei A N. On the p-adic Navier–Stokes equation [J]. Applicable Analysis, 2018, 99(8): 1425-1435.

[19] Lv H X, Qiu K Y, Chen J F. Effective Solution Method of Chemical Reaction Kinetics With Diffuse [J]. Applied Mathematics and Mechanics, 2006, 27(02): 387-394.

[20] Han S W, Cui Z S, Bao L H, et al. Extraction and Measure Based on Target Image [J]. Journal of Shanghai University of Engineering Science, 2007, 27(04):701-710.

[21] Zhang L Y, JI Y B. Checking the Bone Density by Medical Image Based on Alternate Pattern of Random Walk [J]. Journal of Liaoning Shi Hua University, 2010, 30(04): 54-58.